Investigation of Influences of Various Losses on Electromagnetic Torque for Surface-Mounted Permanent Magnet Synchronous Motors

Naomitsu Urasaki, *Member, IEEE*, Tomonobu Senjyu, *Member, IEEE*, and Katsumi Uezato

***Abstract*—Traditionally, vector controlled permanent magnet synchronous motor (PMSM) drives have been performed under the assumption that there is no iron loss, mechanical loss, and stray loss in motors. However, influences of these losses on the vector controlled PMSM drive are hardly evaluated so far. Thus, there is a need to investigate the influences in order to evaluate whether these losses can be neglected. This paper investigates the influences of the iron loss, mechanical loss, and stray loss on surface-mounted PMSM drives. In the first phase, a formulation of the electromagnetic torque taking the various losses into account are developed. In the second phase, the influences of the various losses on the electromagnetic torque under vector control strategy are investigated based on the developed mathematical model. These influences are confirmed by experimental results for torque control of a tested 160 W surface-mounted PMSM.**

***Index Terms*—Electromagnetic torque, iron loss, mechanical loss, permanent magnet synchronous motor, stray loss.**

I. Introduction

TRADITIONALLY, vector controlled ac drives have been performed under the assumption that there is no iron loss in motors. As the employment of vector controlled ac motors, especially induction motor, permanent magnet synchronous motor (PMSM), synchronous reluctance motor has become standard in industrial drives, the improvement of ac motor drives has been important issue. For this reason, several authors have made an attempt to consider the iron loss in vector controlled ac motor drives. Influences of the iron loss on the synchronous reluctance motors has experimentally been investigated [1] and various strategies which compensate the influence of the iron loss have been proposed in [2]–[6]. Influences of iron loss on the flux linkage deviation, its orientation error, and torque deviation of a vector controlled induction motor have analytically been investigated [7] and various compensation strategies have been investigated in [8]–[10]. Although, a number of papers that deal with vector controlled ac motor drive taking the iron loss into account have been published, only a few papers paid attention to PMSM drives [11], [12]. In [11], an iron loss compensation method for PMSM has been proposed based on the basic idea for induction motor in [9]. Although the improvement of the control performance is demonstrated by computer simulations, the influence of the iron loss on the PMSM drive performance does not investigated analytically. In [12], a loss minimization control for PMSM has been developed. Although the iron loss is evaluated as one of the electrical losses of PMSM, there is little mention of the influence of the iron loss on the PMSM drive performance.

In practical situation, there are mechanical and stray losses in addition to the iron loss. However, these losses are usually neglected in vector controlled ac drives. For this reason, influences of the mechanical loss and stray loss are hardly evaluated for so far. Thus, there is a need to investigate influences of these losses as well as the iron loss on vector controlled ac drives in order to evaluate whether these losses can be neglected. In order to analytically evaluate the influence of the iron, mechanical, and stray losses, the mathematical model of surface-mounted PMSM taking these losses into account has been developed in the previous paper [13].

In this paper, influences of the iron, mechanical, and stray losses on PMSM drive performance are investigated based on the developed mathematical model. In the first phase, a formulation of the electromagnetic torque taking the various losses into account are presented. In this mathematical model, a mechanical loss torque and a stray loss coefficient as well as an iron loss resistance are defined. The experimental determination of these values is presented in this paper. In the second phase, the influences of the various losses on the electromagnetic torque under vector control strategy are investigated based on the developed mathematical model. In order to quantitatively evaluate the influences of these losses, a torque generation ratio is utilized. The torque generation ratio is defined as the ratio of actual torque to commanded torque when a loss is neglected [7]. Finally, these influences are confirmed by experimental results for torque control of a tested 160 W surface-mounted PMSM.

Manuscript received January 24, 2001; revised August 14, 2002. This paper was presented at the International Conference on Industrial Electronics, Control and Instrumentation (IECON'00), Nagoya, Japan, October 2000. Recommended by Associate Editor M. A. Rahman.

The authors are with the Department of Electrical and Electronic Engineering, Faculty of Engineering, University of the Ryukyus, Okinawa 903-0213, Japan (e-mail: urasaki@tec.u-ryukyu.ac.jp; b985542@tec.u-ryukyu.ac.jp; uezato@eee.u-ryukyu.ac.jp).

Digital Object Identifier 10.1109/TPEL.2002.807084

II. Formulation of Electromagnetic Torque for PMSM Taking Various Losses Into Account

Fig. 1 shows the d–q axes equivalent circuits of PMSM which are traditionally utilized to consider iron loss [12]. In this circuit, an iron loss resistance R_i is inserted in parallel with the armature inductance. Thus, the d–q axes line currents (i_d, i_q) are divided

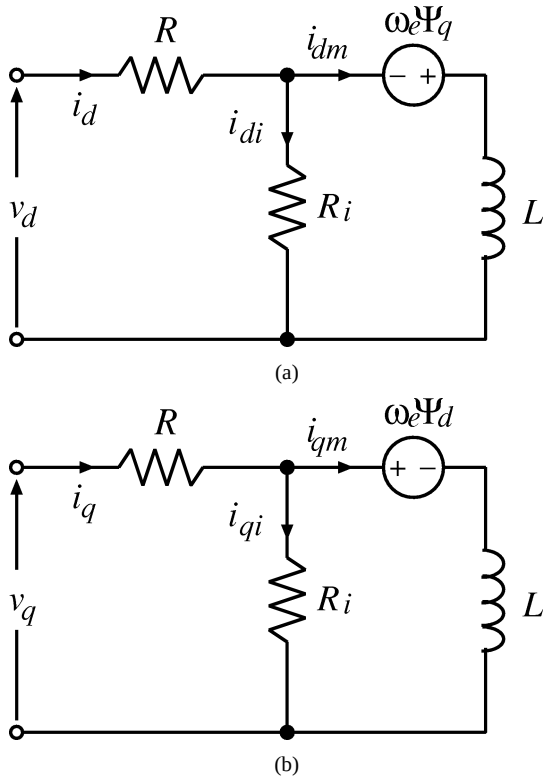

Fig. 1. (a) d-axis and (b) q-axis equivalent circuits for PMSM including iron loss.

into iron loss currents (i_{di}, i_{qi}) and magnetizing currents (i_{dm}, i_{qm}). The voltage equation of these circuits is expressed as

$$\left.\begin{aligned} v_d &= Ri_d + p\Psi_d - \omega_e\Psi_q \\ v_q &= Ri_q + p\Psi_q + \omega_e\Psi_d \end{aligned}\right\} \tag{1}$$

where the flux linkages are given as

$$\left.\begin{aligned} \Psi_d &= Li_{dm} + K_e \\ \Psi_q &= Li_{qm} \end{aligned}\right\} \tag{2}$$

where L is the armature inductance and K_e is the emf coefficient. In steady state condition, the electrical input power P_{in}, derived from (1) and (2), is expressed as

$$\begin{aligned} P_{in} &= v_d i_d + v_q i_q \\ &= R(i_d^2 + i_q^2) + \frac{\omega_e^2(\Psi_d^2 + \Psi_q^2)}{R_i} + \omega_e K_e i_{qm} \end{aligned} \tag{3}$$

where the first and second terms in the right-hand side are the copper loss P_c and iron loss P_i, respectively. The third term refers to the sum of the mechanical loss P_m, stray loss P_s, and mechanical output power P_{out}, that is,

$$\omega_e K_e i_{qm} = P_m + P_s + P_{out}. \tag{4}$$

Since the mechanical output power P_{out} is the product of the mechanical angular velocity ω_m and electromagnetic torque τ, the electromagnetic torque taking the various losses into account can be derived from (4) as

$$\tau = \frac{\omega_e K_e i_{qm} - (P_m + P_s)}{\omega_m} = PK_e i_{qm} - \tau_{ms} \tag{5}$$

where P denotes the number of pole pairs, and τ_{ms} $(=(P_m + P_s)/\omega_m)$ is defined as the loss torque due to the mechanical and stray losses in this paper, i.e., the mechanical and stray losses decrease the electromagnetic torque by τ_m. Because of the presence of the iron loss, the electromagnetic torque is proportion to the q-axis magnetizing current rather than the q-axis line current.

Although the magnetizing currents cannot be detected from the terminal side, they can be obtained [13] by

$$\left.\begin{aligned} i_{dm} &= i_d + \frac{\omega_e L}{R_i}\left(i_q - \frac{\omega_e K_e}{R_i}\right) \\ i_{qm} &= i_q - \frac{\omega_e L}{R_i}\left(i_d + \frac{K_e}{L}\right) \end{aligned}\right\} \tag{6}$$

where the following relation is applied:

$$\left(\frac{\omega_e L}{R_i}\right)^2 \ll 1. \tag{7}$$

This relation means that the iron loss resistance R_i is much greater than the reactance $\omega_e L$.

III. Determination of Iron Loss Resistance and Loss Torque

In order to quantitatively investigate the influence of the various losses on the electromagnetic torque, the iron loss resistance R_i and the loss torque τ_{ms} should be determined in advance.

The additional loss P_l, calculated by subtracting the copper loss P_c and mechanical output power P_{out} from the electrical input power P_{in}, is expressed as

$$P_l = P_i + P_m + P_s = \frac{1}{R_i}\underline{\omega_e^2(\Psi_d^2 + \Psi_q^2)} + (P_m + P_s). \tag{8}$$

Since the mechanical loss P_m and stray loss P_s are almost constant when both rotor speed and load torque are constant, the additional loss P_l can be regarded as the linear function with respect to the square of speed-emf $(\omega_e^2(\Psi_d^2 + \Psi_q^2))$ emphasized with under line in (8). In this situation, the slope of this linear function corresponds to the inverse of the iron loss resistance $(1/R_i)$ and the intercept corresponds to the sum of the mechanical and stray losses $(P_m + P_s)$. Accordingly, the iron loss resistance R_i and the loss torque τ_{ms} is determined by the following procedure.

1) PMSM operates at constant speed and constant load condition.
2) Several input power P_{in}, input voltage V_{rms}, input current I_{rms}, and the output power P_{out}, when d-axis current i_d is changed, are measured. It is noted that the change of the d-axis current makes the flux linkage vary without change of the torque.
3) Using the measurement data by Step 2, the additional loss and the square of speed-emf are calculated as

$$P_l = P_{in} - P_{out} - 3RI_{rms}^2 \tag{9}$$

$$\omega_e^2(\Psi_d^2 + \Psi_q^2) = V_{rms}^2 - 2RP_{in} + 3R^2 I_{rms}^2 \tag{10}$$

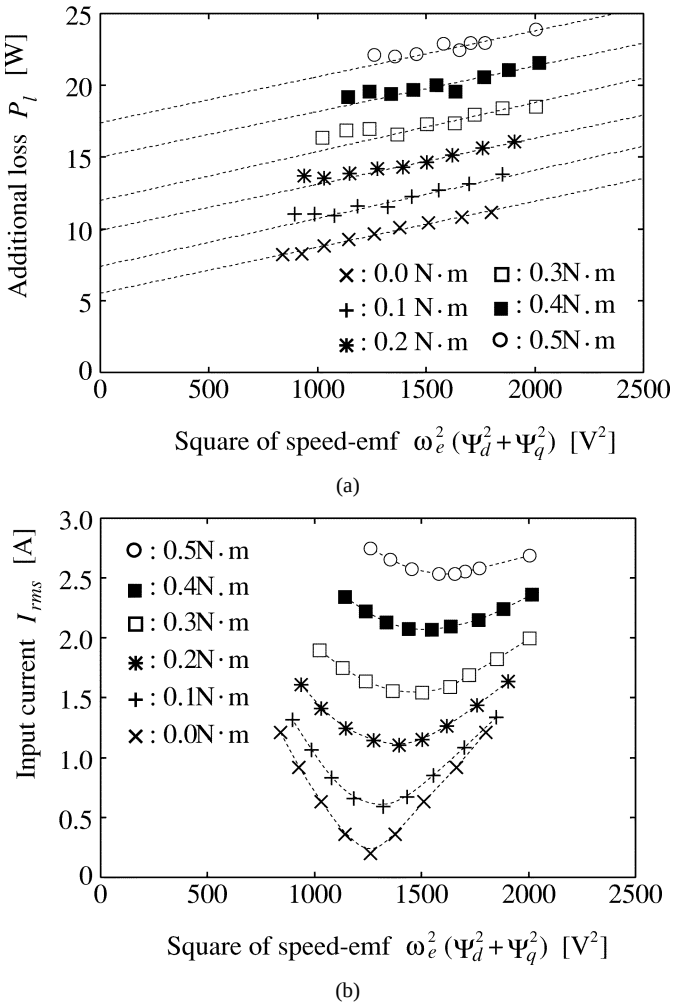

Fig. 2. (a) Additional loss and (b) input current versus square of speed-emf for various load torque at 2500 rpm.

where

$$V_{rms}=\sqrt{v_d^2+v_q^2},\qquad I_{rms}=\sqrt{i_d^2+i_q^2}\Big/\sqrt{3}.$$

4) The characteristic of the additional loss versus the square of speed-emf is plotted. This characteristic theoretically becomes linear.
5) The slope and intercept of this characteristic are calculated with the least squares method.
6) The iron loss resistance R_i is straightforwardly calculated from the inverse of this slope and the loss torque τ_{ms} is calculated by dividing the intercept by the mechanical angular velocity ω_m.

Fig. 2(a) shows the additional loss versus the square of speed-emf obtained from various load conditions at 2500 rpm when the d-axis current is changed from $+2$ A to -2 A. The additional loss decreases with decreasing the d-axis current. In addition, as can be expected from (8), the additional loss is approximately proportional to the square of speed-emf for any load conditions. It is noted that the calculations of the additional loss and square of speed-emf require the information of the armature resistance R. For this reason, the characteristic has been linearized in the neighborhood of the minimum input current I_{rms} in Fig. 2(b), because the armature resistance mismatch is serious at operating points for the increased input current. The iron loss resistance R_i and the loss torque τ_{ms} are determined from the slope and intercept of these linear functions, respectively. In addition, since the slopes for any load conditions are approximately the same, the iron loss resistance is almost constant irrespective of load conditions. By contrast the intercept increases with increasing load torque. The increase of intercept appears to be caused by increased stray loss.

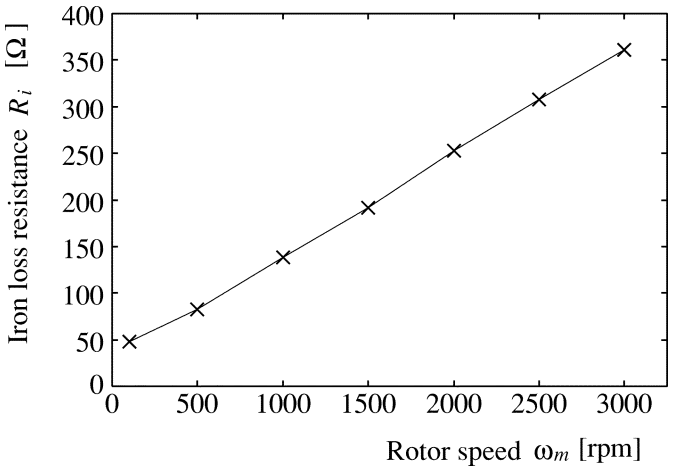

Fig. 3. Iron loss resistance vs. rotor speed.

Similar measurements have been executed in various rotor speeds from 100 rpm to 3000 rpm. Fig. 3 shows the iron loss resistance versus rotor speed. The iron loss resistance is calculated from the inverse of the slope of the linear functions obtained for various rotor speeds. The iron loss resistance increases with increasing the rotor speed. The iron loss resistance for the tested surface-mounted PMSM is determined as shown in the Appendix.

Fig. 4(a) shows the sum of the mechanical loss and stray loss (R_m+R_s) versus the rotor speed for various load torques. In the laboratory setup, a generator is utilized as the load system. The load torque for low speed region is limited due to the low output of the generator, while the load torque for high speed region is limited due to the inverter capability. The sum of the mechanical and stray losses is obtained from the intercept of the linear function between the additional loss and the square of speed-emf. Fig. 4(b) shows the loss torque versus the rotor speed. The loss torque is calculated by dividing the sum of the mechanical and stray losses by the mechanical angular velocity ω_m. The loss torque increases with increasing rotor speed linearly under low speed region because the sum of the losses is proportional to the square of rotor speed as shown in Fig. 4(a). On the other hand, the loss torque for high speed region is almost constant, because the sum of the losses for high speed region is proportional to the rotor speed rather than the square of rotor speed as shown in Fig. 4(a). Since the loss torque for low speed region is comparatively small, the mechanical and stray losses hardly affect the electromagnetic torque under low speed region. For this reason, This paper mainly focuses on the influence of the losses under high speed region. Thus, in order to simplify the analysis, the loss torque is approximated to be constant with respect to

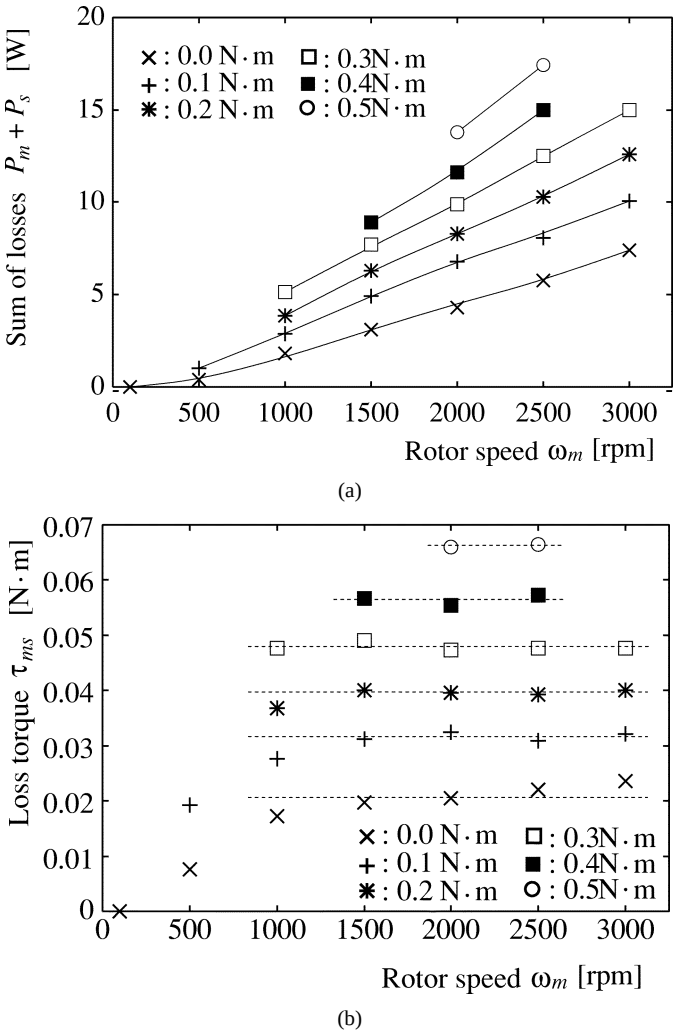

Fig. 4. (a) Sum of the mechanical and stray losses and (b) loss torque versus rotor speed.

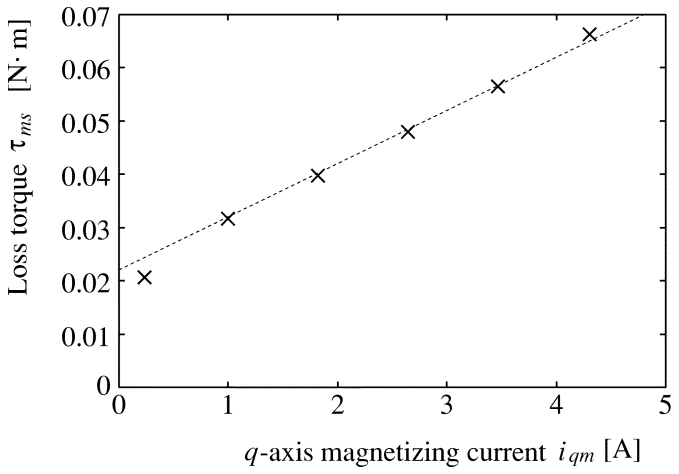

Fig. 5. Loss torque versus q-axis magnetizing current.

rotor speed. Of course, the loss torque should be treated as the function of the rotor speed if an accurate analysis is required.

Fig. 5 shows the loss torque versus q-axis magnetizing current i_{qm}. The loss torque is almost proportional to q-axis magnetizing current. Thus, the loss torque is expressed as a linear function with respect to the q-axis magnetizing current as

$$\tau_{ms} = PK_s i_{qm} + \tau_m. \tag{11}$$

The first term in (11) corresponds to the loss torque increasing with load torque. This term is regarded as the loss torque due to the stray loss. Hence, the stray loss is formulated as the product of the mechanical angular velocity and this loss torque as

$$P_s = \omega_e K_s i_{qm} \tag{12}$$

where K_s is defined as the stray loss coefficient in this paper. The second term in (11) corresponds to the loss torque independent of load conditions. This term is regarded as the loss torque due to the mechanical loss. Hence the mechanical loss is formulated as the product of the mechanical angular velocity and this loss torque as

$$P_m = \omega_m \tau_m \tag{13}$$

where τ_m is defined as the mechanical loss torque in this paper. The stray loss coefficient K_s and the mechanical loss torque τ_m are determined from Fig. 5 as shown in the Appendix. The parameter values listed in the Appendix are valid for the tested PMSM. For other machines, the stray loss coefficient and/or the mechanical loss torque may be a function with respect to the rotor speed.

When the loss torque is formulated by a linear function as (11), the torque equation indicated in (5) is rewritten as

$$\tau = PK_t i_{qm} - \tau_m \tag{14}$$

where K_t $(=K_e - K_s)$ denotes the torque coefficient. The expression of the electromagnetic torque in (14) explicitly indicates the influence of the various losses. The presence of the iron loss causes that the electromagnetic torque is not strictly proportional to the q-axis line current i_q but the q-axis magnetizing current i_{qm}. The mechanical loss decreases the torque by τ_m irrespective of load condition. The stray loss degrades the torque coefficient by K_s. The absence of the stray loss yields that the torque coefficient K_t is equivalent to the emf constant K_e.

IV. Influence of Various Losses on Torque Generation in Vector Control Strategy

In vector control strategy, the distribution of d–q axes currents depends on the torque equation. Then, an improper expression of the electromagnetic torque causes an undesirable torque generation. In this paper, the influence of the iron loss, mechanical loss, and stray loss on the torque generation are investigated based on the developed mathematical model. In order to quantitatively evaluate the influences of these losses, a torque generation ratio (τ/τ^*) is introduced as utilized in the investigation of the influence of the iron loss for induction motors [7]. The torque generation ratio is defined as the ratio of the actual torque τ to the commanded torque τ^* when a certain loss is neglected.

The electromagnetic torque τ_{ni} for neglecting the iron loss is obtained by replacing the q-axis magnetizing current i_{qm} in (14) with the q-axis line current i_q. When the d–q axes currents

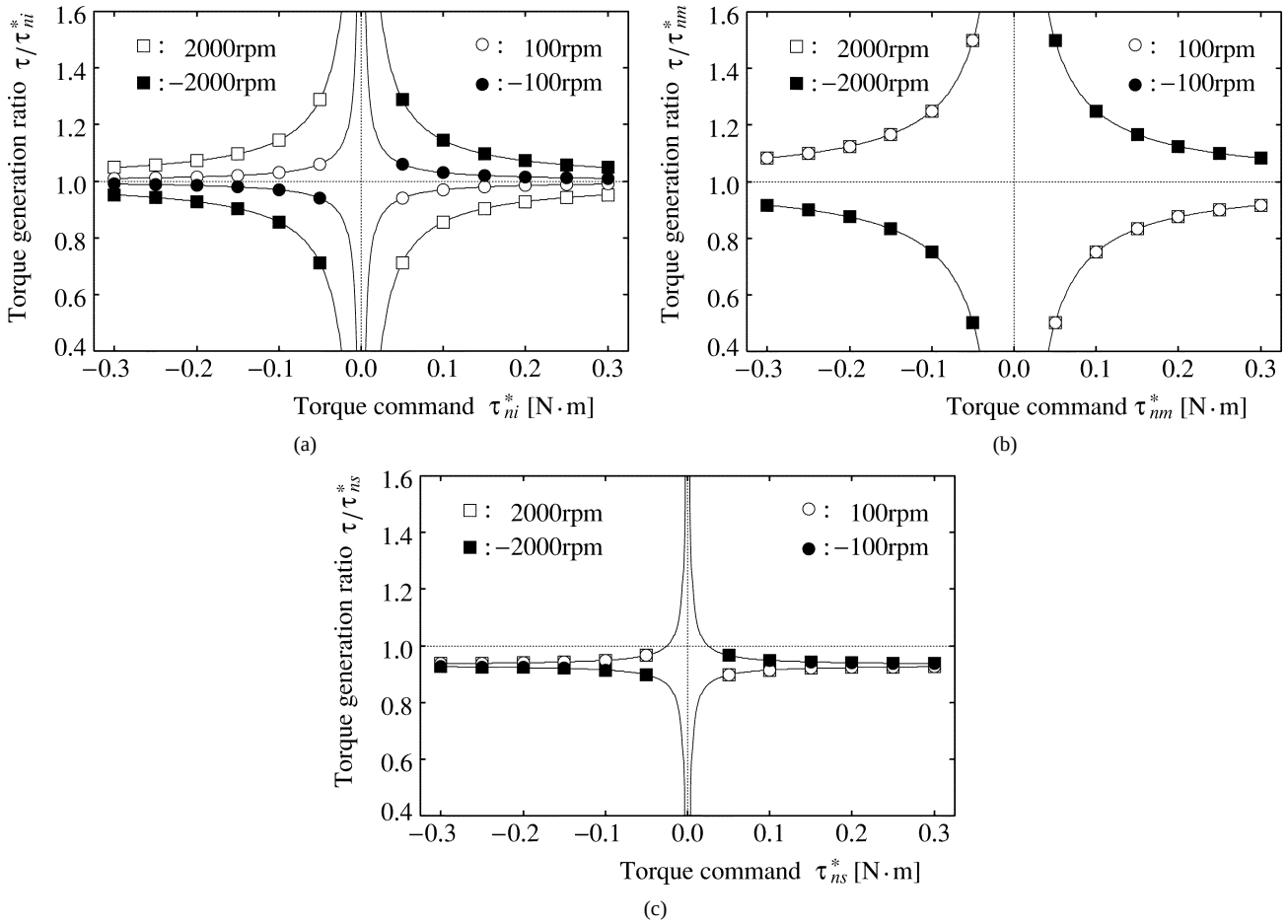

Fig. 6. Torque generation ratio with neglecting: (a) iron loss, (b) mechanical loss, and (c) stray loss.

are distributed corresponding to the torque equation neglecting the iron loss, the torque generation ratio is given as

$$\frac{\tau}{\tau^*_{ni}} = 1 - \frac{\omega_e K_e}{R_i}\frac{PK_t}{\tau^*_{ni}}. \tag{15}$$

The torque equation τ_{nm} for neglecting the mechanical loss is obtained by removing the mechanical loss torque τ_m from (14). Then, the torque generation ratio is derived as

$$\frac{\tau}{\tau^*_{nm}} = 1 - \frac{\tau_m}{\tau^*_{nm}}. \tag{16}$$

The torque equation τ_{ns} for neglecting the stray loss is obtained by replacing the torque coefficient K_t in (14) with the emf coefficient K_e. Then, the torque generation ratio is derived as

$$\frac{\tau}{\tau^*_{ns}} = \frac{K_t}{K_e}\left(1 - \frac{K_e - K_t}{K_t}\frac{\tau_m}{\tau^*_{ns}}\right). \tag{17}$$

Fig. 6 shows the torque generation ratios for the tested PMSM in four quadrant operations. Fig. 6(a) shows the torque generation ratio for neglecting the iron loss. The iron loss decreases the torque in motoring mode ($\omega_m\tau > 0$) and increases in regenerating mode ($\omega_m\tau < 0$). In addition, the effect grows stronger with increasing rotor speed. Fig. 6(b) shows the torque generation ratio for neglecting the mechanical loss. This characteristic is similar to that for neglecting the iron loss. However, this ratio is independent of rotor speed because the mechanical loss torque τ_m for the tested PMSM assumed to be constant. In the strict sense of the word, the torque ratio for 100 rpm approaches 1.0 because of the decrease of the mechanical loss torque τ_m. Fig. 6(c) shows the torque generation ratio for neglecting the stray loss. This characteristic differs from that for neglecting the iron loss or mechanical loss. In other words, the stray loss decreases the torque in both the motoring and regenerating modes except for a very small torque command in regenerating mode. This ratio is also independent of rotor speed due to the constant stray loss coefficient K_s.

V. Experimental Confirmation of Influences of Various Losses

Fig. 7 shows the system configuration for torque control of PMSM. In this system, the block "T/C" converts the torque command τ^* into the q-axis magnetizing current command i^*_{qm} according to the torque equation. This block is most interesting part in this system because the torque control performance strongly depends on the accuracy of this conversion. The d-axis magnetizing current command i^*_{dm} is set at zero. The current controller is made up of a PI controller. The magnetizing currents are obtained through the block "dq/dqm" in which the calculation of (6) is implemented.

Figs. 8–11 show experimental results for torque control of PMSM containing four quadrant operation. A symmetrical step

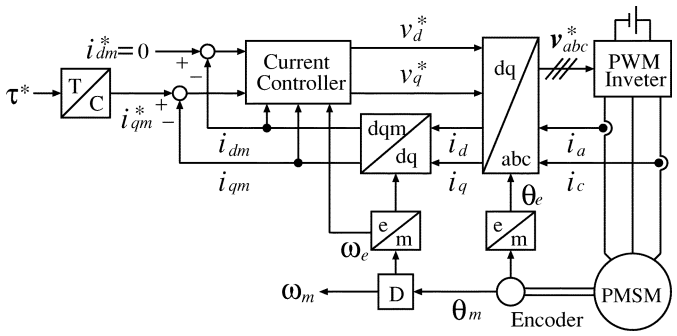

Fig. 7. System configuration for torque control of PMSM.

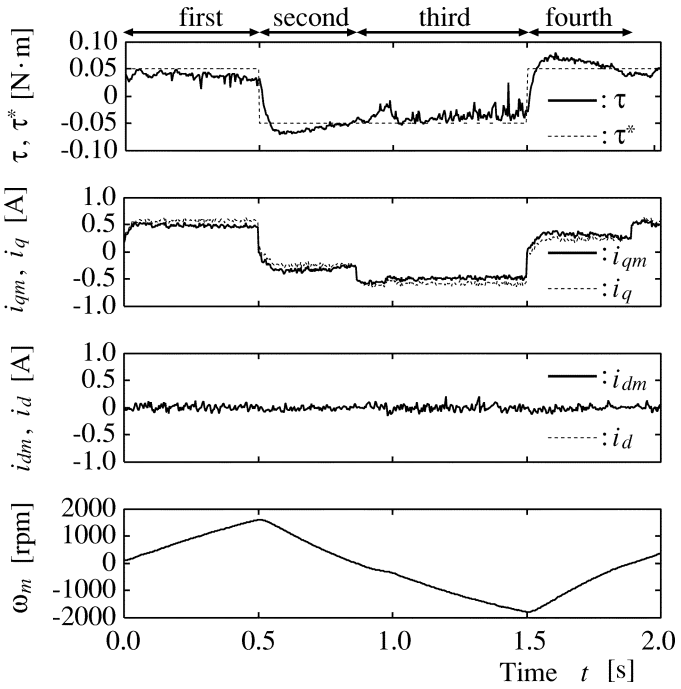

Fig. 8. Torque control performance for neglecting iron loss for no-load condition.

torque whose amplitude is 0.05 N·m is commanded. According to the analytical results shown in Fig. 6, a small torque command causes effective influences on the torque generation.

Fig. 8 shows the torque control performance for neglecting the iron loss, i.e., the electromagnetic torque is directly controlled by the line currents (i_d, i_q). As can be seen form the first trace in Fig. 8, the actual torque τ is smaller than the commanded torque τ^* in motoring (first and third quadrants) mode, and larger in regenerating (second and fourth quadrants) mode. Moreover, the deviation between the actual and commanded torques grows larger with increasing rotor speed. As compared with the commanded torque, the actual torque decreases by 30% at around 2000 rpm and increases by 30% at around -2000 rpm. This experimental results almost agrees with the analytical results shown in Fig. 6(a). The second trace in Fig. 8 shows the q-axis magnetizing current and the q-axis line current. It can be confirmed that the actual torque τ directly depends on the q-axis magnetizing current i_{qm} rather than the q-axis line current i_q. It is noted that the q-axis current for the first quadrant is different from that for the forth quadrant in spite of the same torque command, because the mechanical loss torque component is added to the q-axis current command in motoring mode and reduced in regenerating mode. This is applied to the relationship between the second and third quadrants. It follows from the third trace in Fig. 8 that the d-axis magnetizing current i_{dm} almost agrees with the line current i_d. As can be seen from (6), the iron loss causes that the one axis flux linkage interferes in other axis current. However, since the q-axis flux linkage for the tested PMSM is small, it hardly interferes with the d-axis current. On the other hand, the permanent magnet flux, equivalently the emf constant K_e, for the tested PMSM is comparatively large, the d-axis flux interferes with the q-axis current as shown in the second trace in Fig. 8. The fourth trace in Fig. 8 shows the rotor speed ω_m. It can be confirmed that the acceleration torque in motoring mode degrades, while the braking torque in regenerating mode increases. As a result, the four quadrant speed response becomes asymmetrical against the symmetrical torque command.

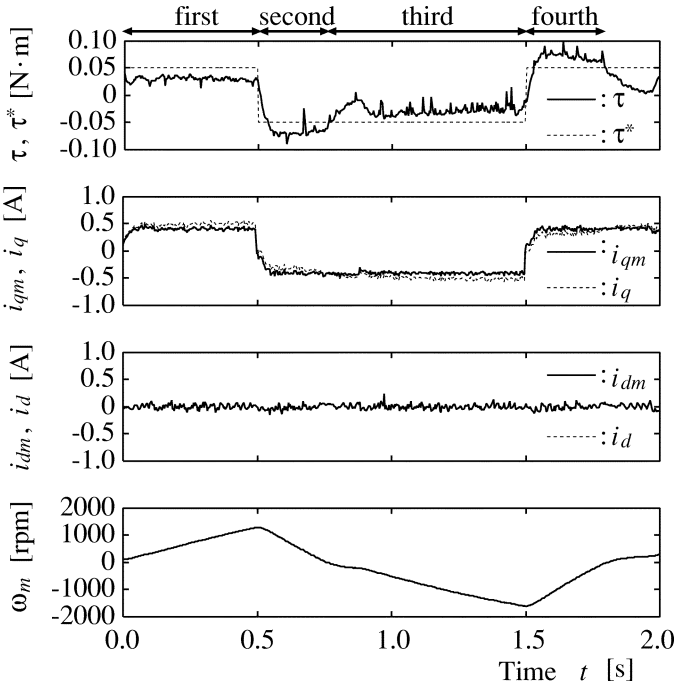

Fig. 9. Torque control performance for neglecting mechanical loss for no-load condition.

Fig. 9 shows the torque control performance for neglecting the mechanical loss, i.e., the torque equation removed the mechanical loss torque τ_m is utilized in the "T/C" block. Since the mechanical loss torque component is omitted form the q-axis current command, both the q-axis currents for the first and fourth quadrants are almost the same. As a result, the actual torque is smaller than the commanded torque in the first quadrant, and larger in the fourth quadrant, respectively. This is applied to the relationship between the second and third quadrants. As indicated in Fig. 6(b), the influence of the mechanical loss on the electromagnetic torque qualitatively agrees with that of the iron loss. The deviation between the actual and commanded torques for Fig. 9 is larger than that for Fig. 8 because the mechanical loss torque τ_m of the tested PMSM is comparatively large. As a result, the four quadrant speed response is severely asymmetrical.

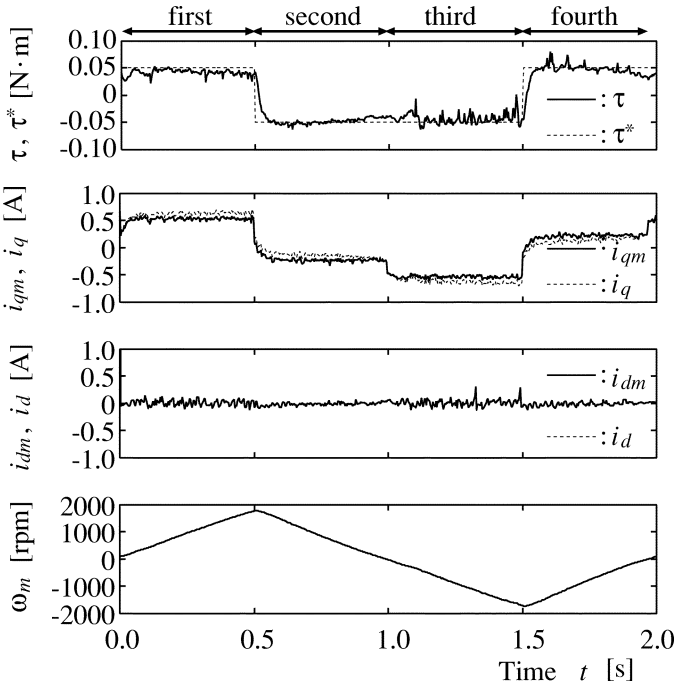

Fig. 10. Torque control performance for neglecting stray loss for no-load condition.

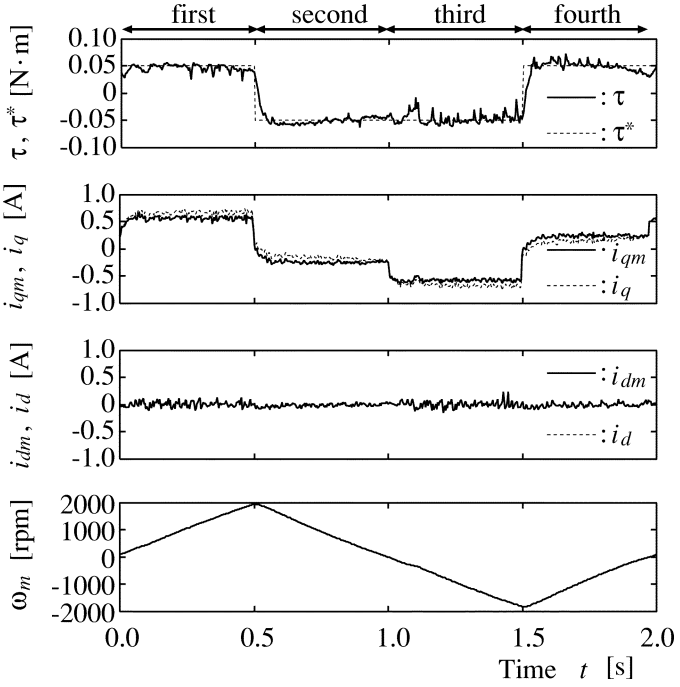

Fig. 11. Torque control performance for considering all the losses for no-load condition.

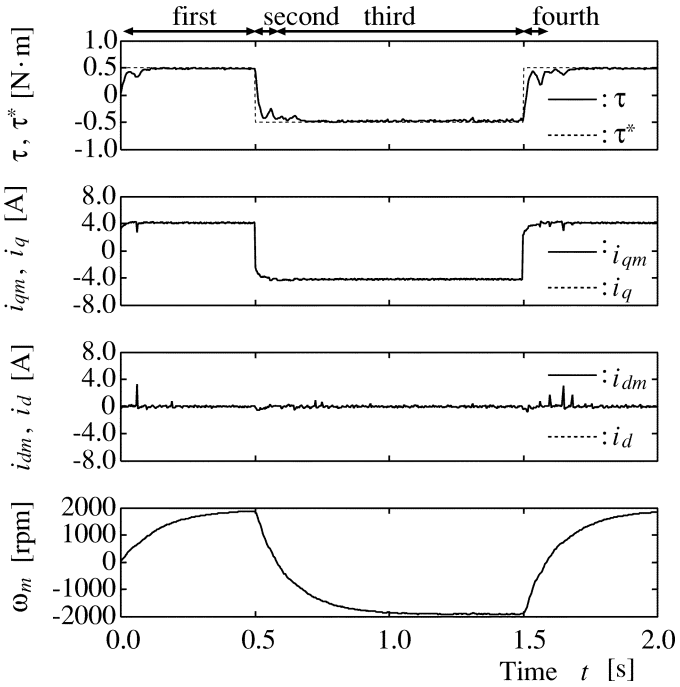

Fig. 12. Torque control performance for neglecting iron loss for load condition.

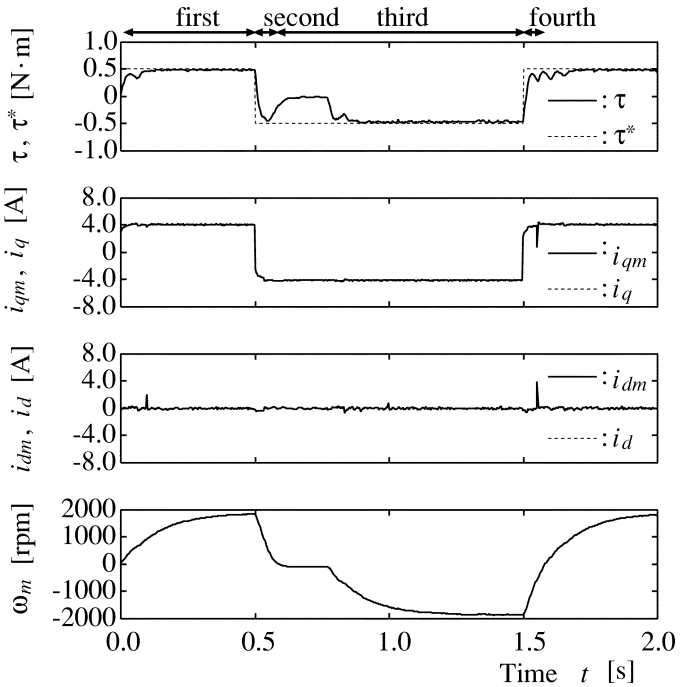

Fig. 13. Torque control performance for neglecting mechanical loss for load condition.

Fig. 10 shows the torque control performance for neglecting the stray loss, i.e., the emf coefficient K_e is used in (14) instead of the torque coefficient K_t. As can be expected from Fig. 6(c), the actual torque is slightly smaller than the commanded torque in both motoring and regenerating modes. As a result, both the acceleration and braking torques are degraded although the four quadrant speed response is symmetrical.

Fig. 11 shows the torque control performance taking all the losses into account. In this case, the actual torque almost agrees with the commanded one. As a result, the four quadrant speed response is symmetrical without degrading both the acceleration and braking torques. Thus, the maximum rotor speed of this figure is larger than that of Fig. 10.

Figs. 12–15 show experimental results for torque control of PMSM containing four quadrant operation. A symmetrical step torque whose amplitude is 0.5 N·m (maximum torque of the tested PMSM) is commanded. From the feature of the load

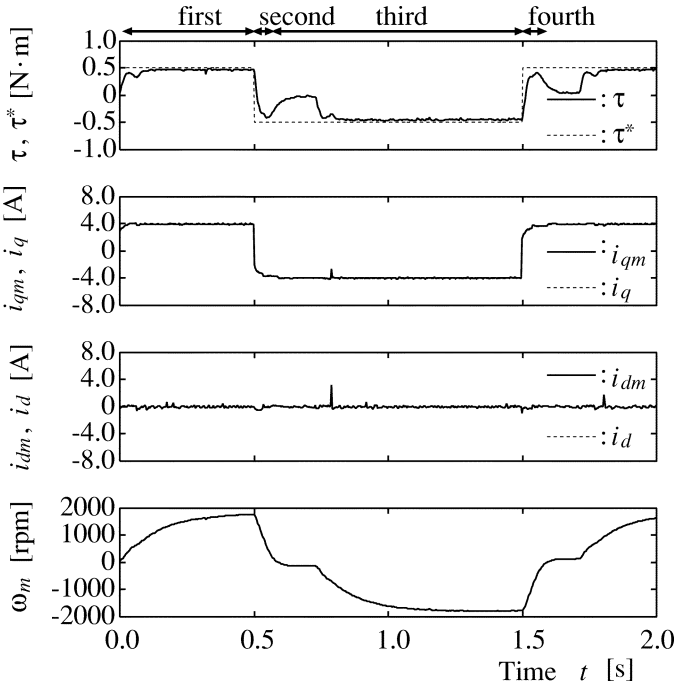

Fig. 14. Torque control performance for neglecting stray loss for load condition.

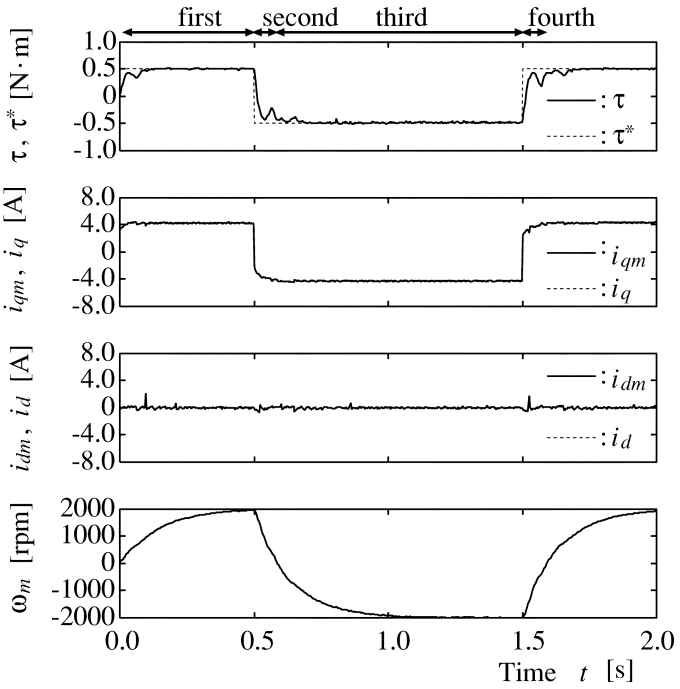

Fig. 15. Torque control performance for considering all the losses for load condition.

system, the load torque increases with increasing rotor speed. In this experiments, the load torque is set at 0.5 N·m at 2000 rpm.

Fig. 12 shows the torque control performance for neglecting the iron loss. As can be expected in Fig. 6(a), the iron loss slightly influences the electromagnetic torque for heavy load condition. It can be confirmed from the fact that the magnetizing current almost agrees with the line current. However, the rotor speed does not reach to 2000 rpm, because the acceleration torque in motoring mode degrades slightly.

Fig. 13 shows the torque control performance for neglecting the mechanical loss. As indicated in Fig. 6(b), since the influence of the mechanical loss is quantitatively larger than that of the iron loss, the degradation of the acceleration torque is large. As a result, maximum rotor speed is degraded. Furthermore, the transition from the second to third quadrant is not a smoothness any longer.

Fig. 14 shows the torque control performance for neglecting the stray loss. Since the stray loss increases with increasing load torque, the influence of the stray loss for heavy load torque is quantitatively larger than that of mechanical loss.

Fig. 15 shows the torque control performance taking all the losses into account. The actual torque almost agrees with the commanded one. Since the acceleration torque is not degraded, the rotor speed reaches to 2000 rpm.

Above experimental results practically agree with the analytical results. Thus, the investigated influences of various losses in this paper are valid.

VI. Conclusion

This paper investigated the influences of the iron loss, mechanical loss, and stray loss on surface-mounted PMSM drive performance. Formulation of the electromagnetic torque taking the various losses into account has been presented. In this mathematical model, the mechanical loss torque and stray loss coefficient as well as the iron loss resistance are defined. The experimental determination of these values is illustrated. The influences of the various losses on the electromagnetic torque has been analytically investigated. The torque generations for neglecting the various losses have quantitatively been evaluated for the tested 160 W surface-mounted PMSM. The iron loss and mechanical loss cause the acceleration torque to decrease in the motoring mode and the braking torque to increase in the regenerating mode. On the other hand, the stray loss degrades both the acceleration and braking torques irrespective of any operation modes. The electromagnetic torque for light load condition is influenced by the iron loss and mechanical loss, while for heavy load condition, it is influenced by the stray loss rather than the iron and mechanical losses. These influences have been confirmed by experimental results for torque control of PMSM.

Appendix
Motor Specifications

rated power	P_n	160 W
armature resistance	R	2.14 Ω
armature inductance	L	0.0065 H
emf coefficient	K_e	0.0658 V · s/rad
number of pole pairs	P	2
iron loss resistance	R_i	$0.53\|\omega_e\| + 30$ Ω
mechanical loss torque	τ_m	$0.02\ \mathrm{sign}(\omega_e)$ N · m
stray loss constant	K_s	0.0045 N · m/A.

REFERENCES

[1] L. Xu, X. Xu, T. A. Lipo, and D. W. Novotny, "Vector control of a synchronous reluctance motor including saturation and iron losses," *IEEE Trans. Ind. Applicat.*, vol. 27, pp. 977–984, Sept./Oct. 1991.

[2] L. Xu and J. Yao, "A compensated vector control scheme of a synchronous reluctance motor including saturation and iron losses," *IEEE Trans. Ind. Applicat.*, vol. 28, pp. 1330–1338, Nov./Dec. 1992.

[3] K. Uezato, T. Senjyu, and Y. Tomori, "Modeling and vector control of synchronous reluctance motors including stator iron loss," *IEEE Trans. Ind. Applicat.*, vol. 30, pp. 971–976, July/Aug. 1994.

[4] S.-J. Kang and S.-K. Sul, "Highly dynamic torque control of synchronous reluctance motor," *IEEE Trans. Power Electron.*, vol. 13, pp. 793–798, July 1998.

[5] A. Vagati, M. Pastorelli, G. Franceschini, and V. Drogoreanu, "Flux-observer-based high-performance control of synchronous reluctance motors by including cross saturation," *IEEE Trans. Ind. Applicat.*, vol. 35, pp. 597–605, May/June 1999.

[6] H.-D. Lee, S.-J. Kang, and S.-K. Sul, "Efficiency-optimized direct torque control of synchronous reluctance motor using feedback linearization," *IEEE Trans. Ind. Electron.*, vol. 46, pp. 192–198, Feb. 1999.

[7] E. Levi, "Impact of iron loss on behavior of vector controlled induction machines," *IEEE Trans. Ind. Applicat.*, vol. 31, pp. 1287–1296, Nov./Dec. 1995.

[8] E. Levi, M. Sokola, A. Boglietti, and M. Patorelli, "Iron loss in rotor-flux-oriented induction machines: Identification, assessment of detuning, and compensation," *IEEE Trans. Power Electron.*, vol. 11, pp. 698–709, Sept. 1996.

[9] T. Mizuno, J. Takayama, T. Ichioka, and M. Terashima, "Decoupling control method of induction motor taking stator core loss into consideration," in *Proc. IPEC'90 Conf.*, Tokyo, Japan, 1990, pp. 69–74.

[10] J. Jung and K. Nam, "A vector control scheme for EV induction motors with a series iron loss model," *IEEE Trans. Ind. Electron.*, vol. 45, pp. 617–624, Aug. 1998.

[11] T. Senjyu, T. Shimabukuro, and K. Uezato, "Vector control of synchronous permanent magnet motors including stator iron loss," *Int. J. Electron.*, vol. 80, no. 2, pp. 181–190, 1996.

[12] S. Morimoto, Y. Tong, Y. Takeda, and T. Hirasa, "Loss minimization control of permanent magnet synchronous motor drives," *IEEE Trans. Ind. Electron.*, vol. 41, pp. 511–517, Sept./Oct. 1994.

[13] N. Urasaki, T. Senjyu, and K. Uezato, "An accurate modeling for permanent magnet synchronous motor drives," in *Proc. APEC'00 Conf.*, New Orleans, LA, 2000, pp. 387–392.

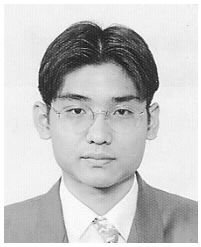

Naomitsu Urasaki (M'98) was born in Okinawa, Japan, on December 21, 1973. He received the B.S. and M.S. degrees in electrical engineering from the University of the Ryukyus, Japan, in 1996 and 1998, respectively.

Since 1998, he has been with the Department of Electrical and Electronic Engineering, Faculty of Engineering, University of the Ryukyus, where he is currently a Research Associate. His research interests are in the areas of modeling and control of ac motors.

Mr. Urasaki is a Member of the Institute of Electrical Engineers of Japan.

Tomonobu Senjyu (M'94) was born in Saga, Japan, on May 2, 1963. He received the B.S. and M.S. degrees in electrical engineering from University of the Ryukyus, Okinawa, Japan, in 1986 and 1988, respectively, and the Ph.D. degree in electrical engineering from Nagoya University, Nagoya, Japan, in 1994.

Since 1988, he has been with the Department of Electrical and Electronic Engineering, Faculty of Engineering, University of the Ryukyus, where he is currently a Professor. His research interests are in the areas of stability of ac machines, advanced control of electrical machines, and power electronics.

Dr. Senjyu is a Member of the Institute of Electrical Engineers of Japan.

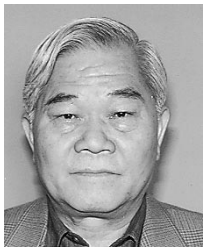

Katsumi Uezato was born in Okinawa, Japan, on February 5, 1940. He received the B.S. degree in electrical engineering from University of the Ryukyus, Okinawa, Japan, in 1963, the M.S. degree in electrical engineering from Kagoshima University, Kagoshima, Japan, in 1972, and the Ph.D. degree in electrical engineering from Nagoya University, Nagoya, Japan, in 1983.

Since 1972, he has been with the Department of Electrical and Electronic Engineering, Faculty of Engineering, University of the Ryukyus, where he is currently a Professor. He is engaged in research on stability and control of synchronous machines.

Dr. Uezato is a Member of the Institute of Electrical Engineers of Japan.